

# Meta-analysis of field scale spatial variability of grassland soil CO<sub>2</sub> efflux: interaction of biotic and abiotic drivers

Szilvia Fóti<sup>a</sup>, János Balogh<sup>b</sup>, Michael Herbst<sup>c</sup>, Marianna Papp<sup>a</sup>, Péter Koncz<sup>a</sup>, Sándor Bartha<sup>d,e</sup>, Zita Zimmermann<sup>b,d</sup>, Cecília Komoly<sup>d</sup>, Gábor Szabó<sup>d</sup>, Katalin Margóczy<sup>f</sup>, Manuel Acosta<sup>g</sup>, Zoltán Nagy<sup>a,b</sup>

<sup>a</sup>MTA-SZIE Plant Ecology Research Group, Szent István University, 2100 Gödöllő, Páter K. u. 1., Hungary, [foti.szilvia@mkk.szie.hu](mailto:foti.szilvia@mkk.szie.hu), [papp.marianna@mkk.szie.hu](mailto:papp.marianna@mkk.szie.hu), [pkoncz@gmail.com](mailto:pkoncz@gmail.com), [nagy.zoltan@mkk.szie.hu](mailto:nagy.zoltan@mkk.szie.hu)

<sup>b</sup>Institute of Botany and Ecophysiology, Szent István University, 2100 Gödöllő, Páter K. u. 1., Hungary, [balogh.janos@mkk.szie.hu](mailto:balogh.janos@mkk.szie.hu)

<sup>c</sup>Agrosphere Institute, IBG-3, Forschungszentrum Jülich GmbH, Jülich, Germany, [m.herbst@fz-juelich.de](mailto:m.herbst@fz-juelich.de)

<sup>d</sup>Institute of Ecology and Botany, MTA Centre for Ecological Research, Alkotmány u. 2-4., H-2163 Vácraót, Hungary, [bartha.sandor@okologia.mta.hu](mailto:bartha.sandor@okologia.mta.hu), [komoly@gmail.com](mailto:komoly@gmail.com), [zimmermann.zita@okologia.mta.hu](mailto:zimmermann.zita@okologia.mta.hu), [szabo.gabor@okologia.mta.hu](mailto:szabo.gabor@okologia.mta.hu)

<sup>e</sup>School of Plant Biology, The University of Western Australia, 35 Stirling Highway, Crawley, WA 6009, Australia

<sup>f</sup>University of Szeged, Department of Ecology, Hungary, 6720 Szeged, Dugonics square 13., [margoczy@bio.u-szeged.hu](mailto:margoczy@bio.u-szeged.hu)

<sup>g</sup>Global Change Research Centre, Academy of Sciences of the Czech Republic, Belidla 986/4a, 603 00 Brno, Czech Republic, [acosta.m@czechglobe.cz](mailto:acosta.m@czechglobe.cz)

Corresponding author: Szilvia Fóti, MTA-SZIE Plant Ecology Research Group, Szent István University, 2100 Gödöllő, Páter K. u. 1., Hungary, [foti.szilvia@mkk.szie.hu](mailto:foti.szilvia@mkk.szie.hu), Tel: +36 28 522 075, Fax: +36 28 410 804

## Abstract

In this study eight temperate grassland sites were monitored for soil CO<sub>2</sub> efflux ( $R_s$ ) and the spatial covariates soil water content (SWC) and soil temperature ( $T_s$ ) at fine scale in over 77 measurement campaigns. The goals of this multisite study were to explore the correlations between environmental gradients and spatial patterns of  $R_s$ , SWC and  $T_s$ , which are not site-specific and to quantify the relevance of biotic and abiotic controls over spatial patterns along increasing vegetation structural complexity. These patterns in water-limited ecosystems in East-Central Europe are likely to be influenced by summer droughts caused by the changing climate.

A consistent experimental setup was applied at the study sites including 75 sampling locations along 15 m circular transects. Spatial data processing was mainly based on variography. Two proxy variables were introduced to relate the site characteristics in terms of soils, water status and vegetation. Normalized SWC (SWC<sub>n</sub>) reconciled site-specific soil water regimes while normalized day of year integrated temperature and vegetation phenology.

A principal component analysis revealed that the progressing closure of vegetation in combination with large  $R_s$  and SWC<sub>n</sub> values, as well as low  $T_s$  and  $R_s$  variability support the detectability of spatial patterns found in both the abiotic and biotic variables. Our results showed that apart from SWC the pattern of soil temperature also had an effect on spatial structures. We detected that when the spatially

## Abbreviations

a - autocorrelation length, c – structural semivariance, DOY – day of year, DOY<sub>n</sub> – normalized day of year, ME - Nash–Sutcliffe model efficiency coefficient, PCA – principal component analysis, psill – partial sill,  $R_s$  – soil CO<sub>2</sub> efflux, sd – standard deviation, SS<sub>Err</sub> - residual sum of squares, SWC – soil water content, SWC<sub>n</sub> - normalized soil water content, TOC – total organic carbon content,  $T_s$  – soil temperature,  $y_0$  – nugget variance

structured variability of  $T_s$  was low, a strong negative correlation existed between SWCn and the spatial autocorrelation length of  $R_s$  with  $r=0.66$  ( $p<0.001$ ). However, for high spatially structured variability of  $T_s$ , occurring presumably at low  $T_s$  in spring and autumn, the correlation did not exist and it was difficult to quantify the spatial autocorrelation of  $R_s$ . Our results are indicative of a potential shift from homogeneity and dominance of biotic processes to an increased heterogeneity and abiotic regulation in drought prone ecosystems under conditions of decreasing soil moisture.

## Keywords

soil CO<sub>2</sub> efflux; variogram; cross-variogram; spatial pattern; principal component analysis

## 1. Introduction

Studies on soil CO<sub>2</sub> efflux ( $R_s$ ) and its driving variables demonstrated differences between spatial and temporal correlations of the observed processes (Chen et al., 2010; Graf et al., 2012; Savva et al., 2013). The spatial structure of soil variables may be affected by numerous factors in a highly complex way due to the spatial and temporal co-variation between the influencing factors. There are still knowledge gaps as to which factors can be responsible for the spatial patterns to be detected and for their actual characteristics.

Spatial variability is often analyzed using the geostatistical approach. The spatial pattern of a variable is usually characterized by the autocorrelation length ( $a$ ) which is a measure of continuity (Savva et al., 2013). The nugget-to-sill ratio or the partial sill (*psill*, named as well as spatially structured variability: the amount of variance structured in space) represent a measure of the spatial dependence or the intensity of the pattern (Chatterjee and Jenerette, 2011). Having low nugget-to-sill ratios (large partial sill, small measurement noise) with a large autocorrelation length is a characteristic of a spatially well-structured variable (Armstrong, 1998; Li et al., 2013).

Savva et al. (2013) reported that the spatial variation of soil water content (SWC) was influenced by the soil microclimate, which simultaneously affected soil water status and soil temperature ( $T_s$ ). The spatial pattern of plant transpiration may further modify this structure (Hu et al., 2011; Savva et al., 2013) and even soil CO<sub>2</sub> efflux could be influenced by transpiration (Balogh et al., 2014), combining the below-ground CO<sub>2</sub> production processes with canopy characteristics. Topographic differences may be relevant drivers of spatial variability of  $R_s$  at the field scale through the co-variation of soil moisture and organic matter content throughout the field (Fang et al., 2009; Hu et al., 2011; Ohashi and Gyokusen, 2007; Xu and Wan, 2008). Continuity or openness of vegetation cover also influences the spatial heterogeneity of  $R_s$  by affecting canopy microenvironment (Chatterjee and Jenerette, 2011; Petrone et al., 2008), plant residue input and spatially heterogeneous root water uptake (Stoyan et al., 2000). Biomass quantity influenced by management practices could also have subsequent effects on  $R_s$  (Koncz et al., 2015).

In addition,  $T_s$  was characterized as a main driver of the temporal variability of  $R_s$  (Chen et al., 2010; Graf et al., 2012; Petrone et al., 2008). However, its co-variation with SWC masks the spatial correlation between  $R_s$  and  $T_s$  (Fóti et al., 2014; Herbst et al., 2009). The lack of a direct effect of  $T_s$  on  $R_s$  in space was not only explained by the relatively small spatial variability of  $T_s$  at field scale (Herbst et al., 2012), but also by the indirect cooling effect of soil water evaporation (Fóti et al., 2014).

Several studies use the parameters of the variograms to compare spatial structures along gradients of explanatory variables.  $R_s$  range of autocorrelation was found to increase and the pattern intensity was found to decrease along an elevation gradient (Chatterjee and Jenerette, 2011). Analysis of the correlations between spatial ranges of annual and perennial plants' covers and different soil properties drew attention to the effect of invasive annual grasses during succession (Parker et al., 2012). The explanatory variable of  $R_s$  spatial patterns would be a spatial flux-controlling factor (Ishizuka et al., 2005), which e.g. determines the variability of  $R_s$ , or influences the stability of the variogram (e.g. in terms of  $a$ , *psill* or goodness of fit). However, environmental factors fluctuate and therefore the spatial patterns vary temporally (Hu et al., 2011), too.

Water limited ecosystems are common in East-Central Europe and are likely to expand due to climate changes (Bartholy and Pongrácz, 2007; IPCC, 2014). In Hungary, precipitation is likely to increase in winter but decrease in summer, which increases the probability of summer droughts (Voss et al. 2002, Räisänen et al. 2004, Frei et al. 2006). Decrease in precipitation together with enhanced evaporation in spring and early summer is very likely to lead to reduced spring/summer soil moisture (Douvillie et al. 2002; Wang 2005). Projected changes will impact the vegetation cover (Mendonça et al., 2010; van der Molen et al., 2011), and the effects of the spatial variability of SWC on  $R_s$  are expected to increase (Gerten et al., 2007). Understanding the links between the influencing factors and  $R_s$  may help in predicting trends in  $R_s$  and related ecosystem responses accompanying climatic changes, or, simply, supporting agriculture to adjust its irrigation and fertilization needs.

The main goal of this multisite study was to identify the common characteristics of the spatial patterns of  $R_s$ , SWC and  $T_s$ , which are not site-specific and can be explained by environmental gradients along the study sites. The specific goals were: (1) to identify the controlling factors of the detectability of fine-scale spatial structures, (2) to identify the drivers of the actual autocorrelation length of  $R_s$ , (3) to describe the potential controlling effects of the vegetation structural complexity on the spatial patterns.

## 2. Materials and methods

### 2.1. Study sites



*Fig. 1. Typical landscapes of the study site subgroups with different levels of productivity (the site actually shown is indicated by bold letters): a: open sandy grasslands with low soil carbon and water content: **O1-O2**, b: closed sandy grasslands with high soil carbon content: **C1-C2**, c: closed sandy grasslands with high soil water content: **W1-W2**, d: closed loess grasslands with high biomass: **B1-B2**.*

The study was conducted in grassland sites with different soil, vegetation and low-intensity management characteristics (Fig. 1) mostly located in Hungary. One of the sites (Beskid Mountains, Czech Republic) was included because of the more humid climate in comparison to the Hungarian dry

grasslands. We split the sites into four largely different subgroups according to their soil organic carbon, soil texture, soil water regime, physiognomy (degree of vegetation closure, height), floristic composition and climatic conditions (Table 1):

1. Fülöpháza-Tece (**O1-O2**): very low TOC, semi-arid, coarse sand, open vegetation, low cover
2. Bugac-Tiszaalpár (**C1-C2**): high TOC, semi-arid, sand, medium/dense cover, medium plant height
3. Mórahalom-Bily Kriz (**W1-W2**): medium/high TOC, humid (due to high groundwater level/high precipitation), sand/sandy loam, dense cover, medium/high plant height
4. Battonya-Isaszeg (**B1-B2**): medium TOC, semi-arid, loam, dense cover, high, vertically well-structured vegetation

The soil characteristics change from very low organic matter content, coarse sand (1.: **O1-O2**) through a much more productive, or semi-arid chernozem type sand (2.: **C1-C2**) to a relatively humid, productive sand/sandy loam soil (3.: **W1-W2**). The fourth group (**B1-B2**) includes two sites with loamy soils in a semi-arid climate. The subgroups from 1 to 4, later on used in the multivariate analysis, therefore represent a systematic increase in biomass, soil water supply, soil fertility and vegetation structural complexity. Therefore, significant differences in the subgroups' spatial parameters and characteristics potentially allow for ecological reasoning. Site characteristics (Table 1) partly correspond to data from Balogh *et al* 2011, Table 1.

#### 1.: Fülöpháza (O1) - Tece (O2)

These two study sites have a very similar botanical composition despite their distant positions in Hungary (Table 1), both are open semi-arid grasslands, but has semi-desert characteristics due to edaphic causes (Fekete *et al.*, 1988). The cover by vascular plants is low, less than 50% on average. Non- vascular plants (*Syntrichia ruralis* and *Cladonia convoluta*) cover amount to about 20%, while the remaining 30% is vegetation-free (Fig. 1(a)). The sites have been abandoned from management more than 30 years ago.

#### 2.: Bugac (C1) – Tiszaalpár (C2)

The Bugac study site (2 ha) is situated in the Hungarian Great Plain (Table 1) and belongs to the Kiskunság National Park (Fig. 1(b)). The vegetation of the sand grassland is diverse (species number over 80, Koncz *et al* 2014). For the last 20 years the site was extensively grazed by cattle, with a stocking density of 0.23-0.58 animal ha<sup>-1</sup>. The sand grassland site at Tiszaalpár has sandy loam soil on loess and with slight alkaline influence. It has been abandoned from sheep grazing in 2011, it is mown once a year since then.

#### 3.: Mórahalom (W1) - Bily Kriz (W2)

The sample site at Mórahalom is situated in the southern part of the Danube-Tisza Interfluvium (Table 1). The species richness is about 80. The vegetation developed in high groundwater level (low water table depths, frequently flooded at springs) conditions and is maintained by a hydrological inflow system within the region (Margóczy *et al.*, 2007). The grassland is managed by extensive mowing and grazing. The grassland site in Bílý Kříž, Czech Republic (Fig. 1(c)) is a yearly mown mountain meadow (Pavelka *et al.*, 2007). The soil texture varies between loamy sand and loam with gravel. The background for grouping **W1** and **W2** sites together, despite of their apparent differences rest on the similarities in their vegetations' structural complexity and in the effective water supply, resulting from the specificities of the water regime of the Hungarian site (water table close to the soil surface).

#### 4.: Battonya (B1) - Isaszeg (B2)

The loess steppe meadow near Battonya is part of the Körös-Maros National Park (Fig. 1(d), Table 1). The species richness is above 200. It is mown once a year. The other xeric temperate loess steppe site is located near Isaszeg. The grassland is not managed, vertically well structured (60-80 cm height), species-rich with several broad- leaved, dicotyledonous and a dwarf shrub species.

Table 1: Site characteristics. 'O1-O2' indicates the first subgroup with open vegetation, 'C1-C2' indicates the second subgroup with more dense vegetation cover, 'W1-W2' indicates the third subgroup with the highest soil water contents and 'B1-B2' indicates the fourth subgroup with the loess soils. Meteorological data were collected directly at the site (O1, C1, C2, W2) or from the nearest meteorological station (O2, W1, B1, B2). The averages were calculated generally for the last 10 years, except for the C2 and B1 sites where 6 (2009-2014), and W2 site where 8 (2007-2014) years' data were available.

	O1-O2		C1-C2		W1-W2		B1-B2	
	O1	O2	C1	C2	W1	W2	B1	B2
<b>Location</b>	46°53'N 19°23'E	47°42'N 19°15'E	46°69'N 19°60'E	46°49'N 19°59'E	46°10'N 19°53'E	49°29'N 18°32'E	46°21'N 20°58'E	47°34'N 19°2'E
<b>Altitude, asl. (m)</b>	130	140	111	103	89	854	99	230
<b>Mean annual temperature (°C)</b>	11.1	10.5	10.4	12.3	11.3	4.9	12.5	9.1
<b>Vegetation period mean temperature (°C)</b>	15.3	15.1	15	16.3	15.7	13.1	16.6	13.1
<b>Annual precipitation (mm)</b>	611	550	562	559	577	1300	601	560
<b>Vegetation period precipitation (mm)</b>	493	410	422	464	477	748	435	417
<b>Soil type (FAO, 1988)</b>	arenosol		chernozem		arenosol	chernozem	chernozem	
<b>Soil texture</b>	sand		sandy loam		sand/sandy loam		loam	
<b>Parent material</b>	sand	sand	sand	sand	sand	mudstones/sandstones	loess	loess
<b>Water table depth (m)</b>	>8	4	4	2	<2	N/A	4	>8
<b>TOC (g kg<sup>-1</sup>)(depth of soil layer, cm)</b>	3.8 (0-10)	17.7 (0-10)	51.5 (0-10)	24	23.3 (0-10)	40 (0-8)	20.3 (0-10)	24.6 (0-10)
<b>Dominant vascular plant species</b>	Festuca vaginata, Stipa borysthenica		Festuca pseudovina, Cynodon dactylon, Poa spp.		Festuca rupicola, Chrysopogon gryllus	Festuca rubra, Nardus stricta	Festuca spp., Teucrium chamaedrys, Galium verum	
<b>Vegetation openness (%)</b>	30-50		3-5		0		0	
<b>Vertical structure</b>	2 layered (cryptogams-annuals and dominant grasses)		2 layered (dominant grasses and grazing tolerant creeping species)		multi-layered (several layers of codominant grasses and forbs)		multi-layered (several layers of codominant grasses and forbs)	
<b>Management</b>	abandoned for >30 years, national park area	abandoned for >30 years, natural reserve area	extensive cattle grazing, national park area	mowing, once a year	occasional grazing/mowing, natural reserve area	mowing, once a year	mowing, once a year	no management, woody plant encroachment

## 2.2. Sampling

In our study 8 temperate grassland sites were monitored for  $R_s$  and the spatial covariates SWC and  $T_s$  at small (a few meters extent) and fine (high spatial resolution) scale in several measurement campaigns with a consistent experimental setup. The sampling scheme consisted of 15 m long circular transects, each with a diameter of 4.77 m, in 75 positions (20 cm distance) each sampled for SWC,  $T_s$  and  $R_s$  (Fig. 2). The advantages of this sampling design include the efficient work flow and the low disturbance level. During the measuring campaigns we intended to avoid short-term effects of precipitation, direct impact of temperature changes and effects due to apparent differences in the elevation or the vegetation structure within a particular transect. The main goal was the description of fine-scale spatial aspects in  $R_s$  under stationary measuring conditions. To avoid fluctuations in the environmental conditions the measurements were started at about noon and for one transect lasted ~ 1.5 hours.

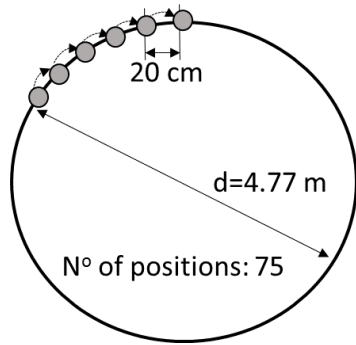


Fig. 2. Schematic figure of the measuring arrangement.

$R_s$  was measured by closed chamber systems (Licor6400, LiCor, Inc. Lincoln, NE, USA and EGM4 PPSystems, Amesbury, USA). The measuring location was changed within the sites in each case and no permanent plots were established. The soil gas exchange chamber was used without collar to minimize soil disturbance and to avoid cutting the roots close to the surface (Davidson et al., 2002, Wang et al., 2005) since both measuring systems performed

well without collars in a comparative study (Pumpanen et al., 2004). Great care was taken during the measurements to ensure non-leaky conditions. All standing biomass was removed 1.5 hours before starting the soil respiration measurements. The litter layer was left intact and ensured proper fit of the chamber to the surface. The 1.5 hours time delay was enough to allow for the dissipation of direct disturbance effects as measured for several hours after the disturbance during pilot investigations (data not shown).

$T_s$  was measured by thermocouples at 0-5 cm soil depth once at each position simultaneously with  $R_s$  near to the gas-exchange chamber. SWC was measured by time domain reflectometry (ML2, Delta-T Devices Co., Cambridge, UK, FieldScout TDR300 Soil Moisture Meter, Spectrum Technologies, IL-USA) for the 0-6 cm soil depth. SWC was measured in the middle of the vegetation-free sample plots in one run (lasting about 10 minutes), after the  $R_s$  measurements to avoid soil disturbance by the instrument's TDR rods.

The total number of sampling campaigns at the 8 sites amounted to 77 between 2003 and 2014 (Table 2), giving a database of  $77 \times 75 \times 3$  data. Data from the C1 site between 2004-2012 have already been published (Fóti et al., 2014, further referred to as 'C1old'). Additional datasets are referred to here as 'C1new'.

*Table 2: Month/Year of measurements, number of measurement campaigns and number of successful soil CO<sub>2</sub> efflux variograms by study sites. 'O1-O2' indicates the first subgroup with open vegetation, 'C1-C2' indicates the second subgroup with more dense vegetation cover, 'W1-W2' indicates the third subgroup with the highest soil water contents and 'B1-B2' indicates the fourth subgroup with the loess soils.*

Site	Month/Year	N° of measurement campaigns	N° of $R_s$ transects included in the analysis
O1-O2	5, 6 and 7/2011; 4 and 5/2012; 4 and 5/2014	18	10
C1-C2	5/2004; 4, 7 and 10/2007; 3, 6 and 8/2010; 6-8/2011; 5-7 and 9/2012; 6/2014	44	33
W1-W2	9-10/2003, 7 and 9/2004, 5-6/2010, 6/2014	10	10
B1-B2	6/2004, 6 and 10/2006, 6/2014	5	3

### 2.3. Data processing

The data analysis consisted of the steps summarized in Fig. 3. The measured data were checked for normality as well as for temporal or large scale spatial trends along the geostatistical analysis (Fox and Weisberg, 2011; Meyer et al., 2014; Pebesma, 2004; R Core Team, 2014; Rossi et al., 1992). Temporal trend in data of the individual campaigns (duration about 1.5 h) was checked for  $T_s$  and  $R_s$ , because these variables were suspected to change rapidly with time, and linear detrending was applied if necessary (Fig. 3. 2<sup>nd</sup>). Normality was checked after any modification of the datasets (Fig. 3. 3<sup>rd</sup>, 4<sup>th</sup> and 8<sup>th</sup>). Variance cloud analysis was performed to detect outlier measurements, excluded from further analysis (Fig. 3. 5<sup>th</sup>: maximum no more than 1-2 measured data were found). After the variogram analysis (Fig. 3. 6<sup>th</sup>), large scale spatial trend was checked for the variables which had an estimated autocorrelation length larger than the spatial extent of the transect ( $a > 4.77$  m, see explanation later, Fig. 3. 7<sup>th</sup>). The spatial trend was removed by linear detrending if the correlation between the data and the x coordinates of the measuring positions was found statistically significant at  $p < 0.05$ . Variogram analysis was repeated for these data (Fig. 3. 9<sup>th</sup>). Datasets not conforming to the 4<sup>th</sup> and 8<sup>th</sup> criteria (Fig. 3) or with the remaining spatial trend (e.g. though the trend was not statistically significant at the  $p < 0.05$  level, it resulted in unbounded variograms) were excluded.

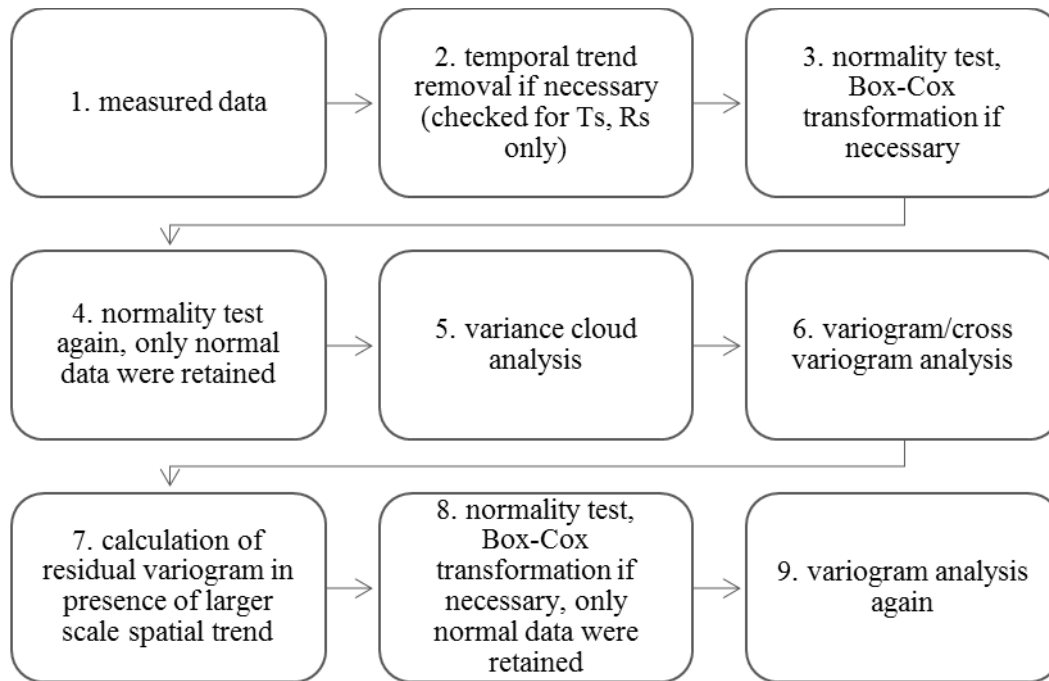


Fig. 3. Data processing.

All variables were standardized to zero mean and unit variance before variography (6<sup>th</sup> step in Fig. 3). This standardization facilitates comparison between different variables (Katsalirou et al., 2010), and helps to avoid that data values may increase or decrease in order of magnitude along Box-Cox transformation. Semivariance ( $\gamma(h)$ ) was calculated according to:

$$\gamma(h) = \frac{1}{2N(h)} \sum_{i=1}^n [z(s_i) - z(s_i + h)]^2, \quad (1)$$

where  $z(s)$  is the value of an abiotic or a biotic variable at a particular location,  $h$  is the average separation distance between data pairs, set to the natural increment (Oliver and Webster, 2014), in this study = 0.2 m, and  $N(h)$  is the number of data pairs separated at a distance of  $h$ .

Exponential, Gaussian and spherical models were fitted to the experimental semivariances against lag distance. The following model parameters were used in the subsequent analysis:  $a$ , the autocorrelation length;  $y_0$ , the nugget variance;  $c$ , the structural semivariance;  $(y_0 + c)$  or 'sill', the total sample

semivariance; *psill*, the ratio of structural variance and total variance, expressed as percentage. The autocorrelation length (*a*) was defined as the distance at which the variogram reaches a plateau. In the case of models with an asymptotic plateau, it is the distance at which 95 % of the total sill is reached. It is calculated from the semivariogram range (*a*<sub>0</sub>) as  $a=3\times a_0$  for the exponential,  $a=3^{0.5}\times a_0$  for the Gaussian, and  $a=a_0$  for the spherical model. As circular transects do not suffer from decreasing number of sample pairs at larger spatial lags, only datasets with autocorrelation lengths larger than 4.77 m (the diameter of the sample circle) were excluded from further analyses.

The criterion for model selection was the residual sum of squares (SS<sub>Err</sub>). The goodness of model fit was quantified by the Nash–Sutcliffe model efficiency coefficient (ME), which is calculated similarly to the coefficient of determination, but ranges from  $-\infty$ , indicating a better prediction of the observed values by the mean than by the model to 1, which points to a perfect match of the observed and modelled data. Only fits with  $ME \geq 0.5$  were accepted at this stage of the analysis. The number of adequate *R<sub>s</sub>* variograms was therefore less than the total number of measured transects (cf. Table 2), the analysis was carried out also to reveal the causes of the failure of the fit (c.f. M&M Section 2.4.) and not only to calculate the parameters of the successful fits.

Cross-variograms were used to investigate the spatial correlation of two variables. Cross-semivariance  $\gamma_x(h)$  was calculated as:

$$\gamma_x(h) = \frac{1}{2N(h)} \sum_{i=1}^n [z(s_i) - z(s_i + h)][z(r_i) - z(r_i + h)], \quad (5)$$

where  $z(s)$  and  $z(r)$  are the two investigated variables. In contrast to direct variograms, cross-variograms could become negative, indicating that the two variables are negatively correlated in space. Positive values indicate positive spatial correlation while values close to zero indicate that they change independently in space. Similarly to experimental variograms, the same theoretical models were fitted to the cross-variograms and the same set of variogram parameters (*y0*, *c*, *sill*, *psill*, *a* and *ME*) were obtained.

After the first runs of the automated data analysis we detected periodicity in the experimental semivariances at the **O1-O2** sites, leading to erroneous fits and total failure of fit. This periodicity was attributed to the spatial pattern of large tussocks and associated large gaps. The middle of the gaps might be dominated by heterotrophic respiration only, whereas in the vicinity of the tussocks autotrophic and heterotrophic respiration occurs. Therefore the analyses of these transects were repeated by increasing the natural lag width to  $2\times h$ , which removed periodicity from the variograms.

## 2.4. Proxy variables and principal component analysis

We investigated a soil moisture gradient (spanning from close to zero to more than 40 % SWC) along the study sites. In order to allow for the comparison of different sites and different measuring campaigns based on their soil water regime and actual soil water status we computed a normalized SWC value:

$$SWC_n = \frac{SWC_{avg} - SWC_{min}}{SWC_{max} - SWC_{min}} \quad (6),$$

where  $SWC_{max}$  and  $SWC_{min}$  were determined as the long term maximum or minimum of repeated SWC measurements site wise, respectively, and  $SWC_{avg}$  represents the actual transect average.

We also investigated the course of *T<sub>s</sub>* and vegetation phenology in the course of the measurement campaigns. For this, we additionally introduced a proxy variable for phenology (DOY<sub>n</sub>), considering growing season start and length as follows:

$$DOY_n = \frac{DOY - DOY_{start}}{DOY_{end} - DOY_{start}} \quad (7),$$

where *DOY* is the actual measurement date,  $DOY_{start}$  and  $DOY_{end}$  determine the beginning and the end of the vegetation period, defined as the first and the last day in the year with a daily average air temperature larger than 5 °C for each site. DOY<sub>n</sub> covered a period between DOY 62 and 325.

Furthermore, Spearman rank correlation was calculated for each measurement campaign between SWC- $R_s$ ,  $T_s$ - $R_s$  and SWC- $T_s$ .

For another step of the analysis we included ME values for all the direct and cross-variograms (also model fits below the threshold 0.5 as applied in Section 2.3.), giving 77 ME values for all of the transects' measured variables (SWC,  $T_s$ ,  $R_s$ ) and variable-pairs (SWC- $R_s$ ,  $T_s$ - $R_s$ , SWC- $T_s$ ). Zero values of ME were chosen for failed fits due to non-normality or large-scale trend. The advantage of including the whole dataset into the analysis (i.e. not only those showing detectable spatial patterns) was the possibility of investigating the circumstances favouring the emergence of spatial patterns. To compare cases with good and failed model fits we used a multivariate analysis (principal component analysis: PCA). To determine the factors causing the success/failure of fits, we correlated the first two principal component scores with the following set of measured and constructed explanatory variables: subgroup, DOYn, averages, standard deviations and coefficients of variation of SWCn,  $T_s$  and  $R_s$ .

### 3. Results

#### 3.1. Structural parameters by variables and subgroup-specific variations

We calculated the averages of the variogram parameters (Table 3) in all of the measurement campaigns. We observed that  $\gamma_0$  was slightly larger for  $R_s$  than for the abiotic variables. In general, an opposite relationship was found for  $c$  and  $psill$ . SWC and  $T_s$  were more strongly dependent spatially (75 %  $psill$  values) than  $R_s$  ( $psill=63$  %). The autocorrelation length was smaller for SWC than for the two other variables. The quality of variogram fits in terms of ME was lower for SWC and  $R_s$  and higher for  $T_s$  (only  $ME \geq 0.5$  were accepted in this analysis).

*Table 3: Average value and standard deviation (sd) of variogram parameters of SWC (%),  $T_s$  (°C) and  $R_s$  ( $\mu\text{mol CO}_2 \text{ m}^{-2} \text{ s}^{-1}$ ) transect measurements: nugget variance ( $\gamma_0$ ), structural semivariance ( $c$ ), total sample semivariance ( $sill$ ), spatially structured variability ( $psill$ ), autocorrelation length ( $a$ ) and goodness of model fit (ME).*

	SWC (%)	$T_s$ (°C)	$R_s$ ( $\mu\text{mol CO}_2 \text{ m}^{-2} \text{ s}^{-1}$ )
nugget variance ( $\gamma_0 \pm sd$ )	0.29±0.31	0.24±0.24	0.39±0.3
structural semivariance ( $c \pm sd$ )	0.71±0.22	0.74±0.28	0.62±0.29
total sample semivariance ( $sill \pm sd$ )	0.98±0.18	0.98±0.19	0.99±0.12
ratio of struct. var. to total var. ( $psill \pm sd$ , %)	75±26	75±24	63±29
autocorrelation length ( $a \pm sd$ , m)	1.08±1.05	1.33±0.82	1.31±1.06
model efficiency coefficient ( $ME \pm sd$ )	0.8±0.14	0.89±0.1	0.83±0.13

Relatively few direct and cross-variogram fits were successful for the driest ecosystem, **O1-O2**, even with a lag distance of  $2 \times h$  (cf. Table 2, Table 4). The best model fits were observed for exponential variograms, in 21 out of the 28 cases, while the Gaussian model provided the best fits for the remaining 7 cases.

*Table 4: Number of accepted variograms by variable, positive and negative Spearman rank correlations and accepted cross-variograms between soil water content (%) and soil  $\text{CO}_2$  efflux ( $\mu\text{mol CO}_2 \text{ m}^{-2} \text{ s}^{-1}$ ): SWC- $R_s$ , soil temperature (°C) and soil  $\text{CO}_2$  efflux:  $T_s$ - $R_s$  and soil water content and soil temperature: SWC- $T_s$ . 'O1-O2' indicates the first subgroup with open vegetation, 'C1-C2' indicates the second subgroup with more dense vegetation cover, 'W1-W2' indicates the third subgroup with the highest water content sites and 'B1-B2' indicates the fourth subgroup with the loess soils.*

	SWC	$T_s$	$R_s$	SWC- $R_s$			SWC- $T_s$			$T_s$ - $R_s$		
				positive	negative	cross	positive	negative	cross	positive	negative	cross
<b>O1-O2</b>	5	13	10	-	2	-	1	1	2	1	6	2
<b>C1-C2</b>	26	35	33	15	-	11	2	19	12	2	11	13
<b>W1-W2</b>	9	9	10	1	1	1	-	3	2	1	-	-
<b>B1-B2</b>	3	4	3	1	-	-	2	1	2	1	-	1

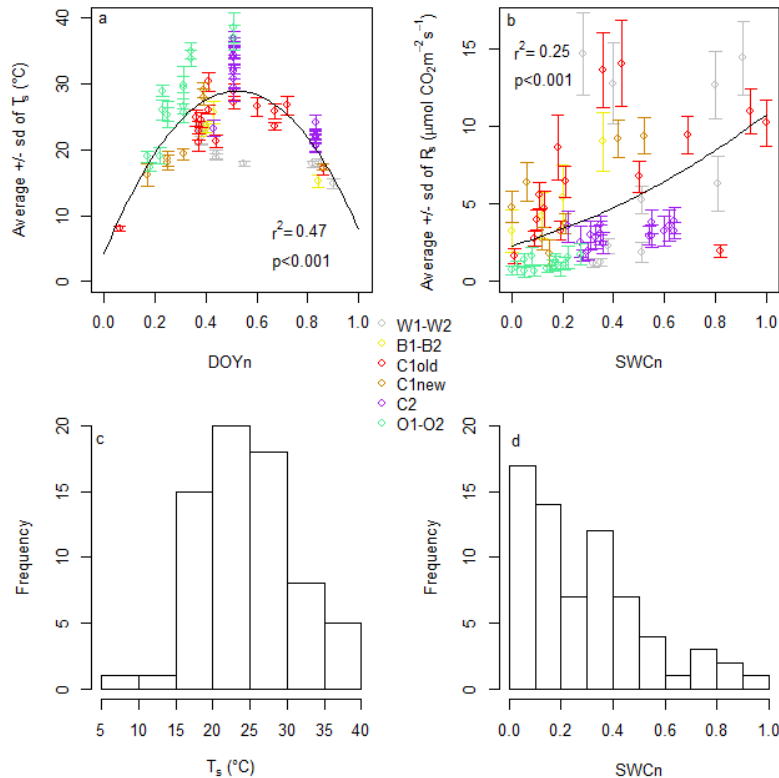
Detailed spatial data about the **C1** site has already been analysed (Fóti et al., 2014). Those datasets were now completed with additional measurements in 2014. The best fits were detected for spherical and Gaussian models while fewer exponential model fits were found to provide the best fit. The main findings based on the correlation and cross-variogram analysis (Table 4) were very similar to those observed at **C1** earlier (Fóti et al., 2014). The spatial correlation was mostly positive between SWC and  $R_s$  while negative correlations were observed between  $T_s$  and  $R_s$  and between SWC and  $T_s$ . However, a few reverse patterns were observed for  $T_s$  vs.  $R_s$  relationship and SWC vs.  $T_s$  relationship.

In the case of the **W1-W2** sites, mostly spherical, and fewer exponential and Gaussian model fits were found to provide the best fit. Of the spatial correlations between variable pairs, two were opposite to the expectations, one negative for the SWC vs.  $R_s$  relationship and one positive for the  $T_s$  vs.  $R_s$  relationship.

In case of the **B1-B2** loess sites, the best variogram fit was mostly spherical. Reverse correlations with positive SWC vs.  $T_s$  and  $T_s$  vs.  $R_s$  correlations were also detected.

### 3.2. Environmental conditions supporting detection of spatial patterns

The measurements over different periods at different sites covered the temporal course of  $T_s$  during the vegetation period, as shown by the distribution of average  $T_s$  values along DOYn (Fig. 4(a)). Observed soil water contents also covered the range of SWCn from about 0 to almost 1 (Fig. 4(b)). Average  $R_s$  values of the transects covered a range between 0.63 and 14.7  $\mu\text{mol CO}_2 \text{ m}^{-2} \text{ s}^{-1}$ . Histograms of the variables (Fig. 4(c-d)) show potential under-sampling at low temperatures and high water supply mainly due to the semi-arid character of most of the study sites, involving a generally higher chance of experiencing low SWC conditions. SWCn rarely reached values close to 1 and the sites were



experiencing frequent draughts.

Fig. 4. Average soil temperature ( $^{\circ}\text{C}$ ) along DOYn (a), average soil  $\text{CO}_2$  efflux ( $\mu\text{mol CO}_2 \text{ m}^{-2} \text{ s}^{-1}$ ) along SWCn (b) and frequency distribution of transect averages of the two main abiotic variables,  $T_s$  (c) and SWCn (d). 'O1-O2' indicates the first subgroup with open vegetation, 'C1 old', 'C1 new' and 'C2' indicate the second subgroup with more dense vegetation cover, 'W1-W2' indicates the third subgroup with the highest soil water contents and 'B1-B2' indicates the fourth subgroup with the loess soils.

In a second step, we investigated the conditions (approximated by available measured and constructed variables, M&M 2.4.) which seemed to be responsible for the goodness of variogram and cross-variogram model fits on experimental SWC,  $T_s$  and  $R_s$  semivariances and cross-semivariances. For this purpose, a principal component analysis was performed on ME values from the fits of the investigated variables and variable pairs (Fig. 5). In the case of the direct variograms, the first and second principal axis explained 40 and 32 % of the variance in the goodness of model fit, respectively. In the case of the cross-variograms, these proportions were 53 % for the first and 29 % for the second principal axis, respectively. The first two axis were responsible for 72 and 82 % of total variability in the goodness of model fits of the direct and cross-variograms, respectively.

Table 5: The relative loadings of the direct and cross-variograms' ME values on the first and second principal components (a), and the signs and p-values of the correlation between the first and second principal components and the explanatory variables (b). \*, \*\* and \*\*\* indicate differences at  $p < 0.1$  and significant differences at  $p < 0.05$  and  $p < 0.01$ , respectively.

(a)				
	Comp. 1	Comp. 2		
ME of SWC	-0.451	0.884		
ME of $T_s$	-0.645	-0.226		
ME of $R_s$	-0.618	-0.41		
ME of SWC- $R_s$	-0.489	0.795		
ME of SWC- $T_s$	-0.569	-0.603		
ME of $T_s$ - $R_s$	-0.661	-		
(b)				
Explanatory variables	Direct variogram PCA component scores		Cross-variogram PCA component scores	
	first axis	second axis	first axis	second axis
SWCn	neg, 0.053*	pos, 0.16	neg, 0.69	pos, 0.94
sd of SWCn	neg, 0.13	pos, 0.01**	neg, 0.4	pos, 0.23
cv of SWCn (%)	pos, 0.31	pos, 0.97	neg, 0.59	pos, 0.79
DOYn	neg, 0.63	pos, 0.06*	pos, 0.81	neg, 0.08*
subgroup	neg, 0.049**	pos, 0.04**	neg, 0.41	neg, 0.78
avg of $T_s$ ( $^{\circ}\text{C}$ )	pos, 0.44	neg, 0.32	pos, 0.56	pos, 0.55
sd of $T_s$	pos, 0.02**	neg, 0.29	pos, 0.84	pos, 0.34
cv of $T_s$ (%)	pos, 0.1	neg, 0.64	neg, 0.49	pos, 0.42
avg of $R_s$ ( $\mu\text{mol CO}_2 \text{ m}^{-2} \text{ s}^{-1}$ )	neg, <0.01***	pos, 0.44	neg, 0.06*	pos, 0.21
sd of $R_s$	neg, 0.02**	pos, 0.53	neg, 0.11	pos, 0.27
cv of $R_s$ (%)	pos, <0.001***	neg, 0.09*	pos, 0.03**	neg, 0.73

The first axis was associated with the fit success: the sign of the loadings was the same for all variables and variable pairs (Fig. 5(a-b), Table 5(a)), which means that probably the same conditions favour the detectability of the patterns irrespective of the type of the variable. The second axis differentiated between the variables/variable pairs with successful fit: the loadings had opposite signs for e.g. goodness of fit of SWC and  $T_s$  or for those of SWC- $R_s$  and SWC- $T_s$  (Table 5(a)), indicating that the conditions favouring the detectability of the patterns may differ, depending on the variable in question. We further analysed these conditions by correlating the first two principal component scores with the above mentioned explanatory variables (Table 5(b)). The cross-variogram fits were generally less affected by any of the factors than the direct variogram fits. We found that the success of model fit for both the direct and cross-variograms (notice that the correlation between the first component score and the explanatory variables (Table 5(b)), and the success of model fit (ME loadings) change in

opposite directions because of the negative loadings!) was negatively correlated to the coefficient of variation of  $R_s$  ( $p < 0.05$ ) and positively correlated to the average of  $R_s$ , with the latter having a low significance of  $p < 0.1$  for the cross-variogram. Furthermore, in the case of direct variograms, an increase in the average and standard deviation of  $R_s$ , SWCn and subgroup membership increased the probability of a successful fit, while the larger standard deviation of  $T_s$  decreased the successful fit probability. These results indicate that the appearance of detectable spatial patterns for both abiotic and biotic variables was typical for higher vegetation cover, increased structural complexity (usually associated with larger heights) and soil characteristics as represented by the subgroup membership. At the same time,  $R_s$  and SWCn values were typically large, while  $T_s$  and  $R_s$  variability were typically low in these cases. The secondary axis refined the results as follows: the second component was associated with increased detectability of SWC pattern in case of increased subgroup membership and standard deviation of SWCn, while the patterns in  $T_s$  and  $R_s$  were better detectable at high coefficients of variation of  $R_s$ . In the case of the cross-variograms, the second component was slightly influenced by DOYn ( $p < 0.1$ , Table 5(b)), large DOYn values supported the link between SWC and  $T_s$  and lower values supported the link between SWC and  $R_s$  patterns. Drought conditions develop at larger DOYn, when the SWC -  $T_s$  patterns are easier detectable and in most cases negatively correlated.

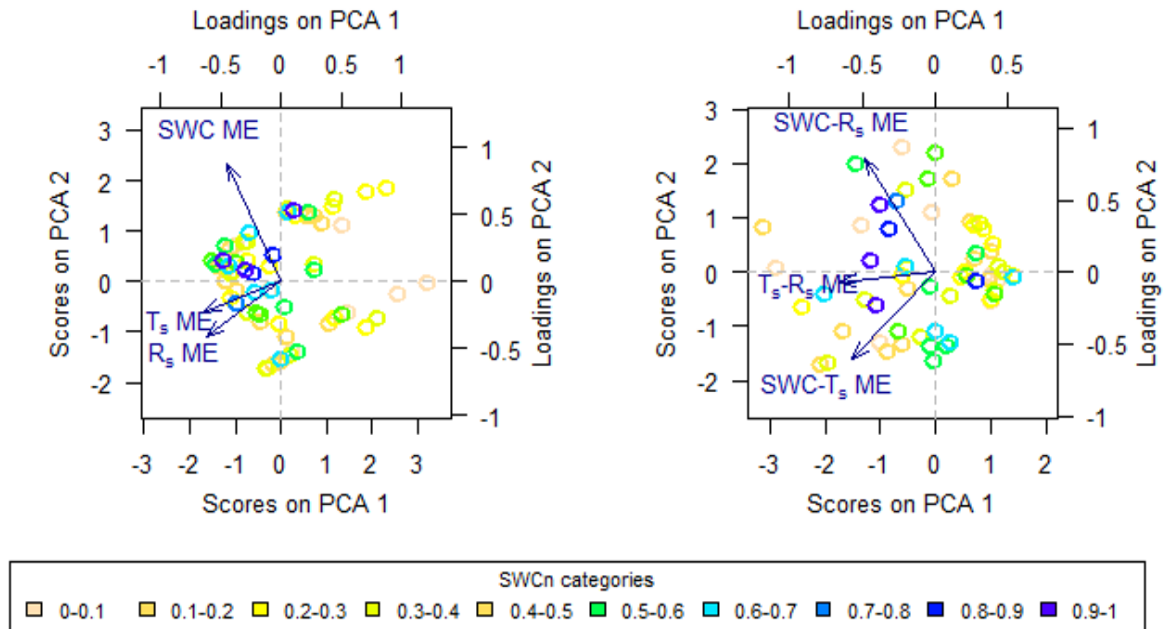


Fig. 5. First two components scores (symbols, bottom and left axis) and component loadings (arrows, top and right axis) of a standardized principal component analysis of ME values of direct (a) and cross-variogram (b) fits. SWC ME,  $T_s$  ME and  $R_s$  ME indicate the goodness of direct variogram model fits, SWC- $R_s$  ME, SWC- $T_s$  ME and  $T_s$ - $R_s$  ME indicate the goodness of cross-variogram model fits. The plot symbol colours correspond to the SWCn categories of the histogram in Fig. 4(d).

### 3.3. Driving factors of spatial characteristics

In a last step we analysed the potential effect of various factors on the spatial autocorrelation of  $R_s$  patterns. We investigated the relationship (linear or quadratic) between several variogram parameters ( $\gamma_0$ ,  $c$ ,  $sill$ ,  $psill$ ,  $a$ ) and transect averages of the measured variables.

The main finding was that the autocorrelation length of  $R_s$  generally decreased with increasing SWCn for all subgroups, except for **W1-W2** (the regression lines serve only for illustration, the significance levels are:  $p=0.014$  for **W1-W2**,  $p=0.22$  for **B1-B2**,  $p=0.013$  for **C1**,  $p=0.096$  for **C2** and  $p=0.64$  for **O1-O2**), despite of the fact that the average  $R_s$  was relatively high in **W1-W2** measurements (cf. Fig. 4(b), grey symbols). High levels of variation were characteristic in the low SWCn ranges, and low levels of variation in the high SWCn ranges (Fig. 6). The spread of data points was more concentrated in the lower left corner of the plot, and no data were found in the upper right corner (marked out by

dashed lines). This is especially important if we consider that spatial detrending (7<sup>th</sup> step in Fig. 3) was required only in the case of 6  $R_s$  datasets, all measured at  $SWCn \leq 0.3$ . This indicates that larger estimated autocorrelation lengths than the diameter of the sample area exclusively occurred at low  $SWCn$ .

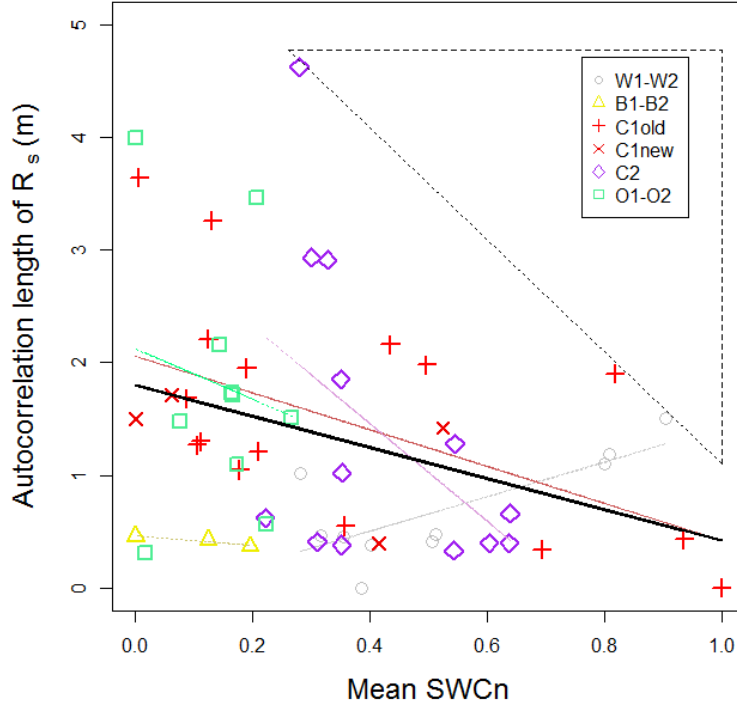


Fig. 6. Autocorrelation length (m) of soil  $CO_2$  efflux vs.  $SWCn$  ( $n = 56$ ). The correlation between  $SWCn$  and  $R_s$  for the whole dataset is statistically significant at  $p < 0.05$  (black line). 'O1-O2' indicates the first subgroup with open vegetation, 'C1 old', 'C1 new' and 'C2' indicate the second subgroup with more dense vegetation cover, 'W1-W2' indicates the third subgroup with the highest water content sites and 'B1-B2' indicates the fourth subgroup with the loess soils. The pale coloured regression lines belong to the symbols with darker tones, green: O1-O2, red: C1, purple: C2, grey: W1-W2, yellow: B1-B2. Note that there are no data within the upper right corner (marked out by dashed lines).

However, the apparent negative correlation between  $a$  of  $R_s$  vs.  $SWCn$  accounted for only 11 % of the total variability of the autocorrelation length at  $p < 0.05$ . We tried to explain a larger part of the variability of the autocorrelation length of  $R_s$  on the basis of other easily measurable factors including  $SWCn$ , average  $T_s$  and sill of  $R_s$  (as a measure of the variability of  $R_s$  of the investigated transect). The results are shown in a conditioning plot (Fig. 7(a)). This combination of constraining factors highlighted more clearly a group of values (upper left panel) at low  $T_s$  in combination with high sill of  $R_s$  (that is high  $R_s$  variability), where the negative correlation between the autocorrelation lengths of  $R_s$  and  $SWCn$  did not exist. This shows that  $R_s$  spatial variability was driven by  $T_s$  and not by  $SWC$  in these cases. The members of this group were mostly transects measured in spring and autumn or at **W1-W2** sites. To link this group of transects more clearly to the effect of  $T_s$  as spatial flux-controlling factor,  $psill$  of  $T_s$  was used to split the data into two groups. The first group was characterized by a strong negative correlation between  $SWCn$  and the autocorrelation lengths of  $R_s$  (Fig. 7(b), left panel), with  $r = 0.66$  at  $p < 0.001$ . The second group with high  $psill$  values of  $T_s$  showed no correlation between the autocorrelation lengths of  $R_s$  and  $SWCn$ . The results indicate that when the spatially structured variability of  $T_s$  was high, occurring presumably at low  $T_s$  in spring and autumn as it can be seen in Fig. 7(a), it was difficult to quantify the spatial autocorrelation of  $R_s$ . Low  $T_s$  was generally coupled with low  $R_s$ , which was already found to be critical for the detection of  $R_s$  spatial patterns (cf. Fig. 5(a) and PCA results).

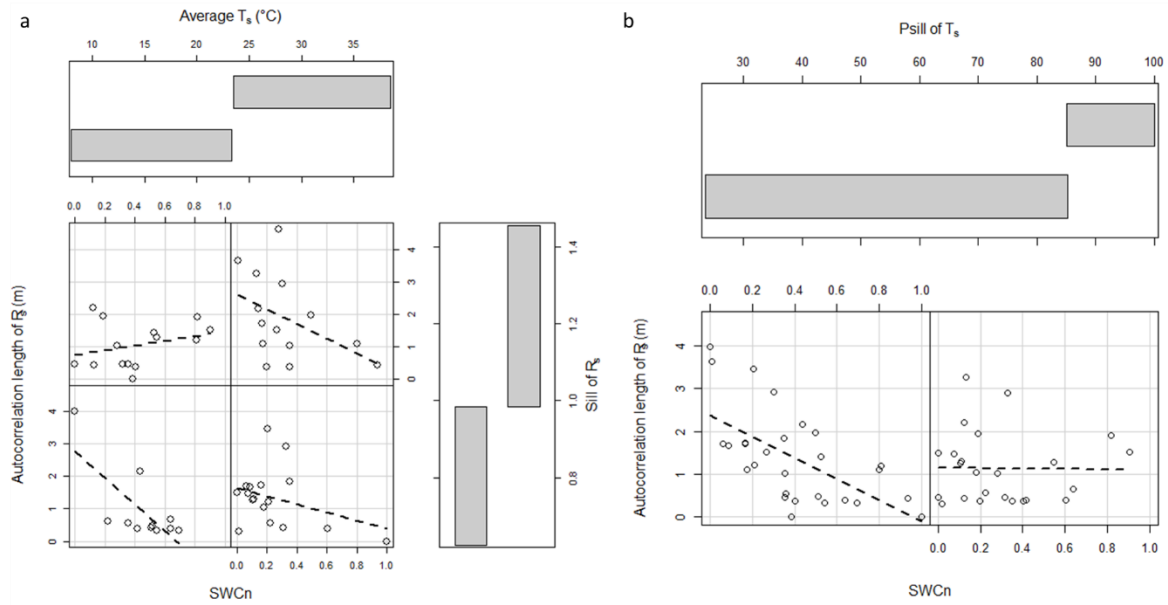


Fig. 7. Conditional plots of multiple factors (a: SWCn, average soil temperature ( $^{\circ}\text{C}$ ), sill of  $R_s$ , b: SWCn, spatially structured variability of  $T_s$ ), which determine the spatial autocorrelation length of  $R_s$ . The autocorrelation length of  $R_s$  dataset is split into the subplots according to the given scales (upper and right for (a), upper for (b)). Regression lines are illustrative except for the left panel in graph (b) with  $r^2=0.43$ ,  $p<0.001$ .

## 4. Discussion

### 4.1. Goodness of model fit is probably under biotic control

The different effect of SWC and  $T_s$  on  $R_s$  in time and space and the inter-correlation between the covariates has already been described (Chen et al., 2010). There is increasing amount of evidence that SWC has a more important effect in space and acts directly on the spatial variability and pattern of  $R_s$ , while  $T_s$  acts indirectly, and consequently less intensively (Kosugi et al., 2007; Mendonça et al., 2010; Yao et al., 2009). SWCn and DOYn were two surrogate variables constructed to relate the datasets of the 77 spatial replicates from 8 sites. DOYn roughly integrated the temperature and the vegetation phenology course along the vegetation period, while SWCn reconciled site-specific water regimes. Courses of  $T_s$  and  $R_s$  averages along these constructed variables proved the applicability of this approach. DOYn, however, was not identified as an important driver of the parameters of the investigated spatial patterns, nor a factor influencing the conditions for the detection of spatial auto- or cross-correlation in SWC,  $T_s$  and  $R_s$ . DOYn had only a slight differentiating effect between the variables/variable pairs with successful fit. Based on the PCA results, obviously  $R_s$  must reach a certain magnitude with decreased variability in the vegetation period, but also before the effects of drought, for the spatial patterns and links between them to become detectable. Our results show that  $T_s$  plays a rather secondary role early in the vegetation period, when the  $T_s$  pattern is stronger. Its variability may even be large enough to affect the  $R_s$  pattern directly while SWC is not limiting yet. When soil moisture content is lower the effect of  $T_s$  on  $R_s$  is more indirect, which corroborates the findings on their profound effects over time (Balogh et al., 2014, 2011; Mäkiranta et al., 2008) rather than in space (Graf et al., 2012; Savva et al., 2013).

### 4.2. Open vegetation is not favourable for the appearance of spatial structures

The four subgroups allowed more detailed observations on the spatial patterns and their controlling factors. For the coarse sandy sites with open vegetation, **O1-O2**, only  $T_s$  vs.  $R_s$  correlations were consistently negative as expected and reported in the literature (Allaire et al., 2012; Almagro et al., 2009; Fóti et al., 2014; Herbst et al., 2009). Furthermore, rather unexpectedly, SWC did not correlate spatially to any other variable and even the appearance of its spatial structure was masked. SWC vs.  $R_s$  spatial correlation was negative in 2 cases while there were no positive correlations, contrary to the

ecosystems with more dense vegetation where the spatial patterns were more complex. Apparently, the given soil conditions of these sites characterised by low total organic matter content and low water holding capacity with the consequent discontinuous vegetation cover may predetermine such deviations. This was the case even when performing the spatial analyses with doubled lag distance. The ratio of rhizospheric/heterotrophic respiration in open communities varies widely in space but it also changes continuously over the vegetation period, hampering the detection of clear spatial patterns (Prolingheuer et al., 2014). It seems that SWC patchiness was less controlled by the vegetation cover than that of  $T_s$ , both being under biotic control in communities with high biomass (Petrone et al., 2008; Saiz et al., 2006; Schlesinger et al., 1990; Veron et al., 2002). Therefore, the background of the apparent  $R_s$  vs.  $T_s$  negative spatial correlation in open grasslands, among others, is probably a direct effect of increased soil surface temperatures in the gaps between the grass tussocks and not an indirect evaporative cooling effect of high SWC on  $T_s$ . The direct effect of radiation on the surface of vegetation gaps may modify directly the patterns of abiotic drivers and biotic variables.

For the **W1-W2** sites we found the other extreme of potential spatial structures. High SWC resulted again in a poor correlation of structures, based on the cross-variograms but in combination with a highly structured and closed vegetation cover. This implies that the spatial scale of the investigated patterns was appropriate. Especially if we consider that almost all of the direct variograms were adequate, but almost no cross-variograms gave acceptable fits. This is probably a result of the ample soil water supply and a lack of environmental constraints (Petrone et al., 2008). This is in accordance with the PCA results, showing that the subgroups with higher structural complexity in combination with ample soil water supply and organic matter content favoured the appearance of spatial structures at the sampling scale. Consequently, the appearance of spatial structures is probably more characteristic of the late than of the early successional stages, and the observed pattern is influenced by the progressing vegetation closure.

The differences in spatial structures within subgroups can be confirmed by differences in variogram models. If there was an accepted model, the exponential type provided most frequently the best fit for **O1-O2**, which indicates that the pattern was generally less structured than at other sites. **W1-W2** and **B1-B2** variograms were mostly of spherical type, pointing to an intermediate spatial structure. For **C1-C2** most variogram models were Gaussian and spherical type, which indicates higher continuity and clearer spatial structure (Armstrong, 1998; Mendonça et al., 2010).

#### 4.3. Temporal constraints of spatial pattern of soil CO<sub>2</sub> efflux

We found that the autocorrelation length or continuity of  $R_s$  depended on SWC<sub>n</sub> but in a highly complex way. The negative correlation between mean SWC and the autocorrelation lengths of  $R_s$  described earlier for **C1** site (Fóti et al., 2014) was verified. However, due to the differences in sites, soils, water status, vegetation periods, measurement dates etc. there was a significant level of variation in spatial autocorrelation of  $R_s$  not explained by SWC. The autocorrelation lengths of  $R_s$  of this group were neither temperature dependent nor limited by DOY<sub>n</sub>, the latter variable being a proxy of the vegetation phenology, describing the growing season course of biomass and greenness development. Other factors, not within the scope of this study may be responsible for the actual patch size of  $R_s$ . We observed that measurements, when spatially structured variability of  $T_s$  was high delimit a group of values, which fit poorly to the regression line between SWC<sub>n</sub> and  $a$  of  $R_s$ . This occurs generally at low average temperatures early or late in the vegetation period. This implies again that  $T_s$  has an effect on spatial structures as well.

#### 4.4. Potential shifts in spatial patterns along decreasing soil moisture

Our results might be relevant to the potential processes linked to global change in drought prone ecosystems (van der Molen et al., 2011). Grasslands have substantial acclimation capacity to climatic variability (Reichstein et al., 2013). However, they can also be exposed to degradation processes due to inappropriate management. Homogenous and less structured biotic processes (in our study, **W1-W2** sites) may consequently become more structured with stronger coupling to the spatial pattern of decreased soil moisture (Saiz et al., 2006; Schlesinger et al., 1990). If the drying process occurs with simultaneous loss of organic matter due to e.g. inadequate land use and/or erosion (Bartha et al., 2011; Reichstein et al., 2013), the coupling effect may diminish or cease completely. This latter aspect needs

further verification, possibly utilizing community succession studies as the process potentially may result in a loss of ecosystem complexity and opening of the vegetation structure (Bartha et al., 2011; Naem, 1998; Schlesinger et al., 1990). Under proper vegetation functioning, the structures and co-structures are present, detectable and show the dominance of the biotic control, therefore the vegetation development and closure in space and time could enhance the interconnections of structures. Uncoupling of these spatial structures (e.g. opposite than expected spatial correlations) indicate an impairment of vegetation functioning including periods when direct effects of abiotic factors determine the interdependencies without the mediating control of biotic factors.

## 5. Conclusion

Our results based on spatial investigations in 8 different grassland sites indicated that ample soil water supply combined with a high complexity in grassland vegetation structure were essential for the emergence and detectability of SWC,  $T_s$  and  $R_s$  spatial patterns. When the patterns were detectable, average  $R_s$  was generally high and its variance was low, compared to the cases when the patterns couldn't be detected. Strong coupling between SWC and  $R_s$  spatial autocorrelation lengths were detected at the drought prone sites.  $T_s$  had an effect on spatial structures in spring and autumn periods when SWC was not limiting. These findings indicate that the autocorrelation length of  $R_s$  was a result of context dependent (valid in only certain domains of the interacting biotic and abiotic drivers) interactions of multiple factors.

As a consequence of global climate change water-limited ecosystems in East-Central Europe are likely to be more exposed to summer droughts. In this study we showed that the expected shifts in the precipitation regime causing reduced soil moisture will affect the spatial patterns of SWC, vegetation cover and subsequently the patterns of  $R_s$  in such a way that a potential loss of homogeneity and biotic regulation and an increase of vulnerability to climatic effects would occur. Our results might be relevant to the potential processes linked to global changes in drought prone ecosystems where opening of the vegetation would potentially result in an impairment of vegetation functioning.

## Acknowledgements

The authors gratefully acknowledge the financial support of the following foundations and research programs, Hungarian national projects (OTKA-PD 100575, OTKA-K 105608) and Animal Change (FP7 266018) EU project. This work was supported by the Ministry of Education, Youth and Sports of the Czech Republic within the National Sustainability Program I (NPU I), grant number LO1415. Szilvia Fóti and János Balogh acknowledge the support of the János Bolyai Research Scholarship of the Hungarian Academy of Sciences. Michael Herbst acknowledges support by the German Research Foundation DFG (Transregional Collaborative Research Centre 32—Patterns inSoil—Vegetation—Atmosphere Systems: Monitoring, modelling and data assimilation).

## References

- Allaire, S.E., Lange, S.F., Lafond, J.A., Pelletier, B., Cambouris, A.N., Dutilleul, P., 2012. Multiscale spatial variability of CO<sub>2</sub> emissions and correlations with physico-chemical soil properties. *Geoderma* 170, 251–260. doi:10.1016/j.geoderma.2011.11.019
- Almagro, M., López, J., Querejeta, J.I., Martínez-Mena, M., 2009. Temperature dependence of soil CO<sub>2</sub> efflux is strongly modulated by seasonal patterns of moisture availability in a Mediterranean ecosystem. *Soil Biol. Biochem.* 41, 594–605. doi:10.1016/j.soilbio.2008.12.021
- Armstrong, M., 1998. Basic linear geostatistics. Springer, New York.
- Balogh, J., Fóti, S., Pintér, K., Burri, S., Eugster, W., Papp, M., Nagy, Z., 2014. Soil CO<sub>2</sub> efflux and production rates as influenced by evapotranspiration in a dry grassland. *Plant Soil*. doi:10.1007/s11104-014-2314-3
- Balogh, J., Pintér, K., Fóti, S., Cserhalmi, D., Papp, M., Nagy, Z., 2011. Dependence of soil

- respiration on soil moisture, clay content, soil organic matter, and CO<sub>2</sub> uptake in dry grasslands. *Soil Biol. Biochem.* 43, 1006–1013. doi:10.1016/j.soilbio.2011.01.017
- Bartha, S., Campetella, G., Kertész, M., Hahn, I., Kröel-Dulay, G., Rédei, T., Kun, A., Virágh, K., Fekete, G., Kovács-Láng, E., 2011. Beta diversity and community differentiation in dry perennial sand grasslands. *Ann. Di Bot.* 1, 9–18. doi:10.4462/annbotrm-9958
- Bartholy, J., Pongrácz, R., 2007. Regional analysis of extreme temperature and precipitation indices for the Carpathian Basin from 1946 to 2001. *Glob. Planet. Change* 57, 83–95. doi:10.1016/j.gloplacha.2006.11.002
- Chatterjee, A., Jenerette, G.D., 2011. Spatial variability of soil metabolic rate along a dryland elevation gradient. *Landsc. Ecol.* 26, 1111–1123. doi:10.1007/s10980-011-9632-0
- Chen, Q., Wang, Q., Han, X., Wan, S., Li, L., 2010. Temporal and spatial variability and controls of soil respiration in a temperate steppe in northern China. *Global Biogeochem. Cycles* 24, 1–11. doi:10.1029/2009GB003538
- Davidson, E.A., Savage, K., Verchot, L., Navarro, R., 2002. Minimizing artifacts and biases in chamber-based measurements of soil respiration. *Agric. For. Meteorol.* 113, 21–37. doi:10.1016/S0168-1923(02)00100-4
- Douville, H., Chauvin, F., Planton, S., Royer, J.-F., Salas-Melia, D., Tyteca, S., 2002. Sensitivity of the hydrological cycle to increasing amounts of greenhouse gases and aerosols. *Clim. Dyn.* 20, 45–68.
- Fang, Y., Gundersen, P., Zhang, W., Zhou, G., Christiansen, J.R., Mo, J., Dong, S., Zhang, T., 2009. Soil–atmosphere exchange of N<sub>2</sub>O, CO<sub>2</sub> and CH<sub>4</sub> along a slope of an evergreen broad-leaved forest in southern China. *Plant Soil* 319, 37–48. doi:10.1007/s11104-008-9847-2
- FAO, 1988. FAO/UNESCO soil map of the world, revised legend with corrections and updates., World Resources Report.
- Fekete, G., Tuba, Z., Melkó, E., 1988. Background processes at the population level during succession in grasslands on sand. *Vegetatio* 77, 33–41.
- Fóti, S., Balogh, J., Nagy, Z., Herbst, M., Pintér, K., Péli, E., Koncz, P., Bartha, S., 2014. Soil moisture induced changes on fine-scale spatial pattern of soil respiration in a semi-arid sandy grassland. *Geoderma* 213, 245–254.
- Fox, J., Weisberg, S., 2011. An {R} Companion to Applied Regression, Second. ed. Sage.
- Frei, C., Schöll, R., Fukutome, S., Schmidli, J., Vidale, P.L., 2006. Future change of precipitation extremes in Europe: Intercomparison of scenarios from regional climate models. *J. Geophys. Res. Atmos.* 111. doi:10.1029/2005JD005965
- Gerten, D., Schaphoff, S., Lucht, W., 2007. Potential future changes in water limitations of the terrestrial biosphere. *Clim. Change* 80, 277–299. doi:10.1007/s10584-006-9104-8
- Graf, A., Herbst, M., Weihermüller, L., Huisman, J.A., Prolingheuer, N., Bornemann, L., Vereecken, H., 2012. Analyzing spatiotemporal variability of heterotrophic soil respiration at the field scale using orthogonal functions. *Geoderma* 181–182, 91–101. doi:10.1016/j.geoderma.2012.02.016
- Herbst, M., Bornemann, L., Graf, A., Welp, G., Vereecken, H., Amelung, W., 2012. A geostatistical approach to the field-scale pattern of heterotrophic soil CO<sub>2</sub> emission using covariates. *Biogeochemistry* 111, 377–392. doi:10.1007/s10533-011-9661-4
- Herbst, M., Prolingheuer, N., Graf, A., Huisman, J.A., Weihermüller, L., Vanderborght, J., 2009. Characterization and Understanding of Bare Soil Respiration Spatial Variability at Plot Scale. *Vadose Zo. J.* 8, 762–771. doi:10.2136/vzj2008.0068
- Hu, W., Shao, M., Han, F., Reichardt, K., 2011. Spatio-temporal variability behavior of land surface soil water content in shrub- and grass-land. *Geoderma* 162, 260–272. doi:10.1016/j.geoderma.2011.02.008

- IPCC, 2014. Climate Change 2014: Mitigation of Climate Change. Contribution of Working Group III to the Fifth Assessment Report of the Intergovernmental Panel on Climate Change. Cambridge University Press, Cambridge, United Kingdom and New York, NY, USA.
- Ishizuka, S., Iswandi, A., Nakajima, Y., Yonemura, S., Sudo, S., Tsuruta, H., Muriyarso, D., 2005. Spatial patterns of greenhouse gas emission in a tropical rainforest in Indonesia. *Nutr. Cycl. Agroecosystems* 71, 55–62. doi:10.1007/s10705-004-5284-7
- Katsalirou, E., Deng, S., Nofziger, D.L., Gerakis, A., Fuhlendorf, S.D., 2010. Spatial structure of microbial biomass and activity in prairie soil ecosystems. *Eur. J. Soil Biol.* 46, 181–189. doi:10.1016/j.ejsobi.2010.04.005
- Koncz, P., Balogh, J., Papp, M., Hidy, D., Pintér, K., Fóti, S., Klumpp, K., Nagy, Z., 2015. Higher soil respiration under mowing than under grazing explained by biomass differences. *Nutr. Cycl. Agroecosystems* 103, 201–215. doi:10.1007/s10705-015-9732-3
- Koncz, P., Besnyői, V., Csathó, A.I., Nagy, J., Szerdahelyi, T., Tóth, Z., Pintér, K., Balogh, J., Nagy, Z., Bartha, S., 2014. Effect of grazing and mowing on the microcoenological composition of semi-arid grassland in Hungary. *Appl. Ecol. Environ. Res.* 1–16.
- Kosugi, Y., Mitani, T., Itoh, M., Noguchi, S., Tani, M., Matsuo, N., Takanashi, S., Ohkubo, S., Rahim Nik, A., 2007. Spatial and temporal variation in soil respiration in a Southeast Asian tropical rainforest. *Agric. For. Meteorol.* 147, 35–47. doi:10.1016/j.agrformet.2007.06.005
- Li, Y., Fu, X., Liu, X., Shen, J., Luo, Q., Xiao, R., Li, Y., Tong, C., Wu, J., 2013. Spatial variability and distribution of N<sub>2</sub>O emissions from a tea field during the dry season in subtropical central China. *Geoderma* 193–194, 1–12. doi:10.1016/j.geoderma.2012.10.008
- Mäkiranta, P., Minkinen, K., Hytönen, J., Laine, J., 2008. Factors causing temporal and spatial variation in heterotrophic and rhizospheric components of soil respiration in afforested organic soil croplands in Finland. *Soil Biol. Biochem.* 40, 1592–1600. doi:10.1016/j.soilbio.2008.01.009
- Margóczy, K., Szanyi, J., Aradi, E., Busa-Fekete, B., 2007. Hydrological background of the dune slack vegetation in the Kiskunság. *Ann. Warsaw Univ. Life Sci. - SGGW. L. Reclam.* 38, 105–113.
- Mendonça, E.D.S., La Scala, N., Panosso, A.R., Simas, F.N.B., Schaefer, C.E.G.R., 2010. Spatial variability models of CO<sub>2</sub> emissions from soils colonized by grass (*Deschampsia antarctica*) and moss (*Sanionia uncinata*) in Admiralty Bay, King George Island. *Antarct. Sci.* 23, 27–33. doi:10.1017/S0954102010000581
- Meyer, D., Dimitriadou, E., Hornik, K., Weingessel, A., Leisch, F., 2014. e1071: Misc Functions of the Department of Statistics (e1071), TU Wien.
- Naem, S., 1998. Species Redundancy and Ecosystem Reliability. *Conserv. Biol.* 12, 39–45.
- Ohashi, M., Gyokusen, K., 2007. Temporal change in spatial variability of soil respiration on a slope of Japanese cedar (*Cryptomeria japonica* D. Don) forest. *Soil Biol. Biochem.* 39, 1130–1138. doi:10.1016/j.soilbio.2006.12.021
- Oliver, M. a., Webster, R., 2014. A tutorial guide to geostatistics: Computing and modelling variograms and kriging. *Catena* 113, 56–69. doi:10.1016/j.catena.2013.09.006
- Parker, S.S., Seabloom, E.W., Schimel, J.P., 2012. Grassland community composition drives small-scale spatial patterns in soil properties and processes. *Geoderma* 170, 269–279. doi:10.1016/j.geoderma.2011.11.018
- Pavelka, M., Acosta, M., Marek, M. V., Kutsch, W., Janous, D., 2007. Dependence of the Q<sub>10</sub> values on the depth of the soil temperature measuring point. *Plant Soil* 292, 171–179. doi:10.1007/s11104-007-9213-9
- Pebesma, E.J., 2004. Multivariable geostatistics in S: the gstat package. *Comput. Geosci.* 30, 683–691.
- Petrone, R.M., Chahil, P., Macrae, M.L., English, M.C., 2008. Spatial variability of CO<sub>2</sub> exchange for riparian and open grasslands within a first-order agricultural basin in Southern Ontario. *Agric.*

- Ecosyst. Environ. 125, 137–147. doi:10.1016/j.agee.2007.12.005
- Prolingheuer, N., Scharnagl, B., Graf, a., Vereecken, H., Herbst, M., 2014. On the spatial variation of soil rhizospheric and heterotrophic respiration in a winter wheat stand. *Agric. For. Meteorol.* 195–196, 24–31. doi:10.1016/j.agrformet.2014.04.016
- Pumpanen, J., Kolari, P., Ilvesniemi, H., Minkkinen, K., Vesala, T., Niinistö, S., Lohila, A., Larmola, T., Morero, M., Pihlatie, M., Janssens, I., Yuste, J.C., Grünzweig, J.M., Reth, S., Subke, J.-A., Savage, K., Kutsch, W., Østreng, G., Ziegler, W., Anthoni, P., Lindroth, A., Hari, P., 2004. Comparison of different chamber techniques for measuring soil CO<sub>2</sub> efflux. *Agric. For. Meteorol.* 123, 159–176. doi:10.1016/j.agrformet.2003.12.001
- Räisänen, J., Hansson, U., Ullerstig, a., Döscher, R., Graham, L.P., Jones, C., Meier, H.E.M., Samuelsson, P., Willén, U., 2004. European climate in the late twenty-first century: Regional simulations with two driving global models and two forcing scenarios. *Clim. Dyn.* 22, 13–31. doi:10.1007/s00382-003-0365-x
- R Core Team, 2014. R: A Language and Environment for Statistical Computing. R Foundation for Statistical Computing, Vienna, Austria.
- Reichstein, M., Bahn, M., Ciais, P., Frank, D., Mahecha, M.D., Seneviratne, S.I., Zscheischler, J., Beer, C., Buchmann, N., Frank, D.C., Papale, D., Rammig, A., Smith, P., Thonicke, K., van der Velde, M., Vicca, S., Walz, A., Wattenbach, M., 2013. Climate extremes and the carbon cycle. *Nature* 500, 287–295. doi:10.1038/nature12350
- Rossi, R.E., Mulla, D.J., Journel, A.G., Franz, E.H., 1992. Geostatistical tools for modeling and interpreting ecological spatial dependence. *Ecol. Monogr.* 62, 277–314.
- Saiz, G., Green, C., Butterbach-Bahl, K., Kiese, R., Avitabile, V., Farrell, E.P., 2006. Seasonal and spatial variability of soil respiration in four Sitka spruce stands. *Plant Soil* 287, 161–176. doi:10.1007/s11104-006-9052-0
- Savva, Y., Szlavecz, K., Carlson, D., Gupchup, J., Szalay, A., Terzis, A., 2013. Spatial patterns of soil moisture under forest and grass land cover in a suburban area, in Maryland, USA. *Geoderma* 192, 202–210. doi:10.1016/j.geoderma.2012.08.013
- Schlesinger, W.H., Reynolds, J.F., Cunningham, G.L., Huenneke, L.F., Jarrell, W.M., Virginia, R. a, Whitford, W.G., 1990. Biological feedbacks in global desertification. *Science* (80-. ). 247, 1043–1048. doi:10.1126/science.247.4946.1043
- Stoyan, H., De-Polli, H., Robertson, G., 2000. Spatial heterogeneity of soil respiration and related properties at the plant scale. *Plant Soil* 222, 203–214.
- van der Molen, M.K., Dolman, A.J., Ciais, P., Eglin, T., Gobron, N., Law, B.E., Meir, P., Peters, W., Phillips, O.L., Reichstein, M., Chen, T., Dekker, S.C., Doubkova, M., Friedl, M. a., Jung, M., van den Hurk, B.J.J.M., de Jeu, R. a. M., Kruijt, B., Ohta, T., Rebel, K.T., Plummer, S., Seneviratne, S.I., Sitch, S., Teuling, A.J., van der Werf, G.R., Wang, G., 2011. Drought and ecosystem carbon cycling. *Agric. For. Meteorol.* 151, 765–773. doi:10.1016/j.agrformet.2011.01.018
- Veron, S.R., Paruelo, J.M., Sala, O.E., Lauenroth William K., 2002. Environmental Controls of Primary Production in Agricultural Systems of the Argentine Pampas. *Ecosystems* 5, 625–635. doi:10.1007/s10021-002-0145-1
- Voss, R., May, W., Roeckner, E., 2002. Enhanced resolution modelling study on anthropogenic climate change: changes in extremes of the hydrological cycle. *Int. J. Climatol.* 22, 755–777. doi:10.1002/joc.757
- Wang, W.J., Zu, Y.G., Wang, H.M., Hirano, T., Takagi, K., Sasa, K., Koike, T., 2005. Effect of collar insertion on soil respiration in a larch forest measured with a LI-6400 soil CO<sub>2</sub> flux system. *J. For. Res.* 10, 57–60. doi:10.1007/s10310-004-0102-2
- Xu, W., Wan, S., 2008. Water- and plant-mediated responses of soil respiration to topography, fire,

and nitrogen fertilization in a semiarid grassland in northern China. *Soil Biol. Biochem.* 40, 679–687. doi:10.1016/j.soilbio.2007.10.003

Yao, Z., Wolf, B., Chen, W., Butterbach-Bahl, K., Brüggemann, N., Wiesmeier, M., Dannenmann, M., Blank, B., Zheng, X., 2009. Spatial variability of N<sub>2</sub>O, CH<sub>4</sub> and CO<sub>2</sub> fluxes within the Xilin River catchment of Inner Mongolia, China: a soil core study. *Plant Soil* 331, 341–359. doi:10.1007/s11104-009-0257-x